

Deformation micromechanics of a thermoplastic-thermoset interphase of epoxy composites reinforced with polyethylene fiber

P. I. GONZALEZ-CHI

Unidad de Materiales, Centro de Investigación Científica de Yucatán, A. C., Calle 43 No. 130, Col. Chuburná de Hidalgo, CP 97200, Mérida, Yucatán, México
E-mail: *ivan@cicy.mx*

R. J. YOUNG

Manchester Materials Science Centre, University of Manchester/UMIST, Grosvenor Street, Manchester, M1 7HS, UK

The polyethylene fibre is one of the strongest man-made materials; its strength is based on its high crystallinity order. Nevertheless, due to the Polyethylene chemical nature, it shows a low reactivity, which limits its use for composite materials, especially with thermoset matrices like the Epoxy resin. The present work uses Raman Spectroscopy to monitor the loading and failure of a thermoplastic-thermoset interface. Pull-out specimens were prepared with Spectra 1000 Polyethylene fibre embedded in a epoxy resin block; the fibre extraction was performed in a stepwise fashion and with the aid of a micro-Raman, spectra were taken along the interface through out the whole process. The technique allowed to measure the interface strength and to monitor the propagation of the debonding front up to total failure. Some results correspond to specimens where the interface was improved by changing the surface chemistry of the thermoplastic fibre to make it more compatible to the thermoset matrix. © 2004 Kluwer Academic Publishers

1. Introduction

Traditional thermoset matrices are reinforced with ceramic fibres like carbon or glass fibre. These composites are well known by their performance; nevertheless, the brittleness of their reinforcement limits their final applications. The use of thermoplastic fibres, due to their greater toughness could lead to materials with complete new properties, opening a whole new range of applications for thermoset based composites.

The composite design using these materials is focused on creating a good interface by increasing the attraction between both materials and improving the wetting or the mechanical anchoring, even promoting the chemical bonding. Deformation micromechanics is the best way to assess the changes occurring on the interface: using model composites is possible to measure the interfacial resistance (the interface is directly deformed).

One of the oldest micromechanical tests used to evaluate the interfacial shear strength of a fibre/matrix system is the Single Fibre Pull-out Test [1–4] which has been used for the interfacial characterisation of many systems, its popularity is based on the relative simplicity of specimen preparation and test procedure. Nevertheless, the reliability of the reported results for this test is questionable not only due to the limited analy-

sis of the stress distribution, but also, due to the test procedure, which has not been standardised [5, 6]. The general procedure consists of partially embedding a single filament in a resin disk, cylinder, block or droplet. By applying a force to the free fibre in the axial direction, the fibre is pulled out from the resin. During the test, the load applied to the fibre is continuously monitored until either the interface or the fibre fails.

The conventional analysis for this test only assumes yielding with a constant shear stress along the fibre/matrix interface; this is far from what it happens in a real situation. It ignores any stress concentration, the lack of linearity between the maximum force required for pull-out and the embedded length [7, 8], it does not consider the effects of stable fibre debonding and the subsequent effects of interfacial friction [9–11]. These misleading approaches produce an unrealistic estimate of the Interfacial Shear Strength (ISS).

Raman spectroscopy had been used to monitor the debonding process in pull-out test [12–18], clearly evidencing the progressive failure of the fibre/matrix interface during the test. The debonding of the reinforcing PE fibre can be detected with Raman spectroscopy by following the 1127 cm^{-1} band, which corresponds to the symmetric C-C stretching mode. This band shifts

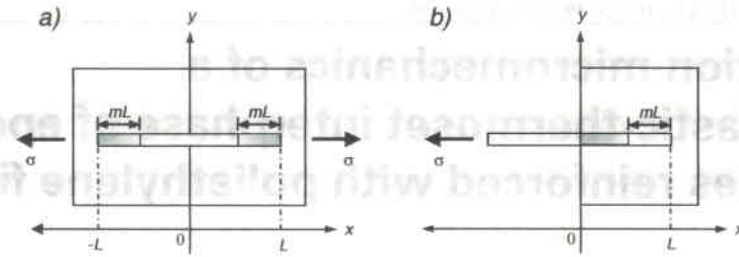


Figure 1 Debonding front (mL) for (a) shear lag-fragmentation and (b) pull-out model.

linearly to the applied stress [19–21]. The rate of shifting of this band, better known as the Raman Stress Sensitivity Factor ($dv/d\sigma$), is used to transform the band position into stress [22, 23]. The typical procedure consists on calculating the $dv/d\sigma$, from the Raman band shifting of a free fibre by applying a series of increasing known stresses. When a composite is deformed, the stress applied is transmitted to the embedded fibre through the interface. Then by taking spectra along the surface of the embedded fibre and transforming the position of the 1127 cm^{-1} band to stress, it is possible to measure not only the stress transfer along fibre but also the extent of the debonding region.

The initial stages of the debonding process are characterised by the elastic response of the interface. Interfacial failure generates a debonding front, which travels along the embedded fibre creating a partially debonded region near the free fibre. Eventually, the fibre fully debonds and is pulled out against frictional forces. The partial debonding theory proposed by Piggott [24] for the Fragmentation Test can easily be modified for the Pull-out Test [25]. The original work considers a fibre fragment with a $2L$ length, fully embedded in the resin which is deformed in tension. In the pull-out test, the fibre is deformed not the resin. This difference reverses the way in which the debonding front propagates. In fragmentation, the debonded region is defined as having a mL length from the fibre tip. In pull-out this region corresponds to the fully bonded one. The debonding front travels from the point where the fibre enters the resin block to the embedded tip (Fig. 1).

The partial debonding model can easily be adapted to fit the corresponding stress/position profiles obtained by Raman spectroscopy. Equations 1 and 2 represent the stress and the ISS at the debonded region respectively [24–27].

$$\sigma_{fe} = \sigma - \frac{2\tau_{rp}x}{r} \quad (1)$$

$$\tau_{rp} = -\mu\sigma_f \quad (2)$$

where σ_{fe} is the stress at the debonded region, τ_{rp} is the ISS at the debonded region, σ is the stress on the free fibre, σ_f is the residual stress, μ is the frictional coefficient, r is the fibre radius, and x is the position along the fibre surface.

In the case of the elastic region, the Equations that describe the stress and the ISS along the fibre

are 3 and 4:

$$\sigma_{fc} = \sigma_{fi} \left[\frac{\sinh\left(\frac{n(L-x)}{r}\right)}{\sinh(nsm)} \right] \quad (3)$$

$$\tau = \frac{n\sigma_{fi}}{2} \left[\frac{\cosh\left(\frac{n(L-x)}{r}\right)}{\sinh(nsm)} \right] \quad (4)$$

with

$$n^2 = \frac{2G_m}{E_f \ln(R/r)} \quad (5)$$

$$s = \frac{L}{r} \quad (6)$$

$$\sigma_{fi} = \sigma - \frac{2\tau_{rp}(1-m)L}{r} \quad (7)$$

The stress at the transition point between the debonded and bonded regions can be calculated with Equation 7:

where σ_{fc} is the stress at the bonded region, τ is the ISS at the bonded region, σ_{fi} is the stress at the transition point between the bonded and the debonded region, n is a non-dimensional parameter, s is the aspect ratio, L is the embedded length, m is a constant, R is the volume fraction parameter, G_m is the matrix shear modulus, and E_f is the fibre modulus.

2. Experimental

2.1. The matrix

Commercial grades of epoxy resin are usually a combination of different chemicals. In the present case, the epoxy resin used was Ciba-Geigy 5052 [28] which is basically a Novolac epoxy resin mixed with 34–42% of 1,4-Butanediol diglycidylether which acts as an epoxy diluent to control the viscosity of the resin during cure. The corresponding hardener is also a mixture of 50–60% of 4,4'-Diamino-3-3'-dimethyldicyclohexylmethane, 35–45% of Isophorone diamine and 1–5% 2,4,5-Tris(dimethylaminomethyl)-phenol.

The resin was mixed with 38% by weight of hardener, degasified *in vacuo* and allowed to cure at room temperature (RT) for at least 4 weeks in a controlled-environment room ($25^\circ \pm 1^\circ\text{C}$ and $50 \pm 2\%$ relative humidity). The mechanical properties of the resin cured at RT were: Modulus, $3.45 \pm 0.1\text{ GPa}$, Elongation at break, $1.9 \pm 0.4\%$ and Shear Yield Strength, $41.8 \pm 2\text{ MPa}$ [29].

2.2. The fibres

Two commercial fibres were used: Spectra 1000 with no surface treatment (US) and Plasma Treated Spectra 1000 (TS—the exact treatment is proprietary), both provided by Allied-Signal, Petersburg, USA. The fibre diameters were $34.2 \pm 7.2 \mu\text{m}$ for US and $32.4 \pm 5.4 \mu\text{m}$ for TS [30]. The manufacturer describes the mechanical properties of these fibres as having a modulus of 170 GPa and a maximum elongation of 2.7% (at a strain rate of 0.02 s^{-1}). The Raman Stress Sensitivity Factor, $(d\nu/d\sigma)$, was 5.9 ± 1 and $5.6 \pm 0.4 \text{ cm}^{-1}/\text{GPa}$ respectively [30].

An oxidative acid etching treatment changed the surface chemistry of the fibres. The US fibre was treated with a Chromic Acid Mixture and the TS fibre was post-treated with concentrated Sulphuric Acid [31], in this case, the synergic effect of both treatments was analysed. A section of the PE yarn (US or TS) was soaked in the respective chemical for a specific temperature and time (US 1 min at RT and TS 5 min at 70°C). Immediately, the Yarn was rinsed with tap water (3 times) and then with distilled water (2 times) and finally with acetone. The fibre was dried overnight *in vacuo* at Rt. These two treated fibre batches: Untreated Spectra 1000 with Chromic treatment (UC) and Plasma Treated Spectra 1000 with Sulphuric post-treatment (TC) were stored in a controlled atmosphere room ($23^\circ \pm 1^\circ\text{C}$ and $50 \pm 2\%$ humidity).

Any surface treatment could affect the mechanical performance of the fibre by weakening its structure (molecular bonds break) [32]. Nevertheless, in the present case no strong evidence was found that the applied acid etching treatments significantly affected the mechanical properties of the fibres or their Raman Spectra [33]. They behave (UC and TC) similar to their non-treated counterpart fibres (US, TS) [30].

2.3. The test procedure

The pull-out specimens were prepared using silicone rubber frames [13] with a rectangular cavity of about $8 \times 5 \times 4 \text{ mm}$ (Fig. 2). A razor blade cut of about 2 mm deep was made on one side of the mould wall. The mould was flexed to open the cut to allow the introduction of a fibre and then released to grip it. The desired embedded length was obtained by drawing the fibre through the cut. The frame holding the fibre was

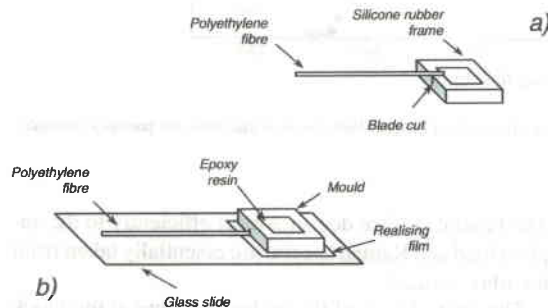


Figure 2 Mould to prepare a pull-out specimen: (a) Fibre clamped to a rubber frame and (b) mould setting for the epoxy resin.

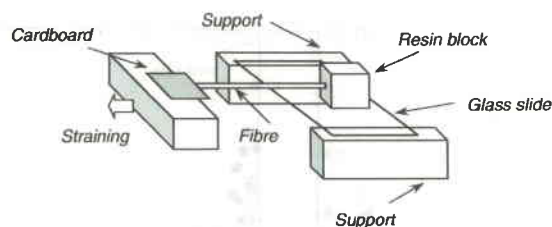


Figure 3 Pull-out specimen cemented to the straining rig.

stuck to a glass slide with a release film; the pool was then filled up with the epoxy resin and allowed to cure. Specimens were prepared with a range of embedded lengths from 800 to $2500 \mu\text{m}$.

To test the specimens, the mould was carefully released and then the free fibre tied and glued to a small piece of cardboard, leaving about 2 cm of free fibre. The specimen was then cemented to a straining rig (Fig. 3) and this placed on the microscope stage of a Renishaw 1000 micro-Raman Spectrophotometer. The laser (He-Ne/25 mW) was focused on the fibre surface. Then, Raman spectra of the 1127 cm^{-1} band were taken along the fibre. The scanning was from the embedded fibre tip to the fibre in air using a 5s exposure at intervals of about $25 \mu\text{m}$. The free fibre was deformed in steps of about $100 \mu\text{m}$ by moving the cardboard-grip away from the resin block using a micrometer (Fig. 3). The mapping along the fibre was repeated after each pull. This procedure was repeated until the fibre was pulled out from the resin block. The band position (ν) of the 1127 cm^{-1} Raman band was plotted against position (x) along the PE fibre surface and using the $d\nu/d\sigma$ from the free fibre, this distribution was transformed into stress vs. position [34].

3. Results and discussion

In order to have a clearer description of the fibre stress profiles, certain terminology needs to be defined. The *Block edge*, is the resin boundary at the point where the fibre enters the resin block. The *Fibre tip*, corresponds to the interface around the embedded fibre end. The *Fibre body* is the fibre region between the block edge and the fibre tip. These terms will be used to describe the fibre interface failure at each region.

3.1. Pull-out debonding process

Fig. 4 shows an example of the stress profiles for a TS fibre. This is a typical stress distribution for a pull-out specimen. The profiles have been divided in three sections: Fig. 4a corresponds to the elastic response of the system, Fig. 4b to the partial-debonding response and finally, Fig. 4c to the frictional response of the fibre as it is pulled out. After interfacial failure, several important facts regarding to the debonding process, applicable to all the specimens tested, can be generalised.

The stress level on the free fibre was calculated from their Raman Band shifts. It increased steadily up to a maximum level, which in the present case is 0.62 GPa, and it remained more and less constant even if the rig

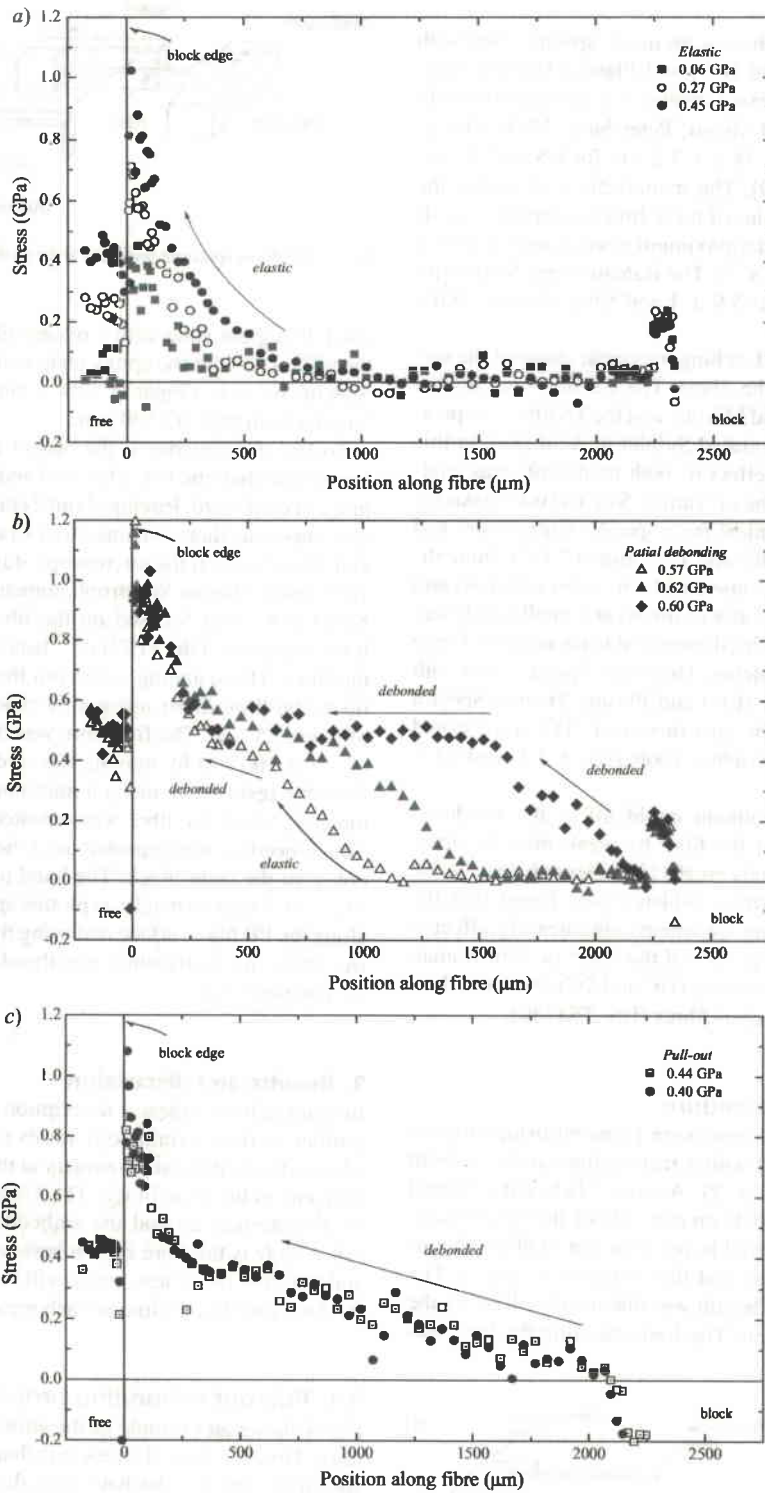


Figure 4 Debonding process for a Pull-out specimen. Plasma Treated Spectra 1000 Fibre (TS): (a) Fully bonded interface, (b) partially debonded interface, and (c) fully debonded interface.

blocks where further separated. PE is a viscoelastic material and relaxes naturally after deformation. The stress on the free fibre, near to the block edge surface is lower than the average stress on the rest of the free fibre (e.g., the profile at 0.45 GPa). This could be caused by surface damage on the fibre during the specimen manufacture.

The broken surface does not react efficiently to the applied load and Raman spectra are essentially taken from the fibre surface.

The stress levels of the embedded fibre at the block edge are very high in comparison with the stress levels at the free fibre. The interface behaves as an irreversible

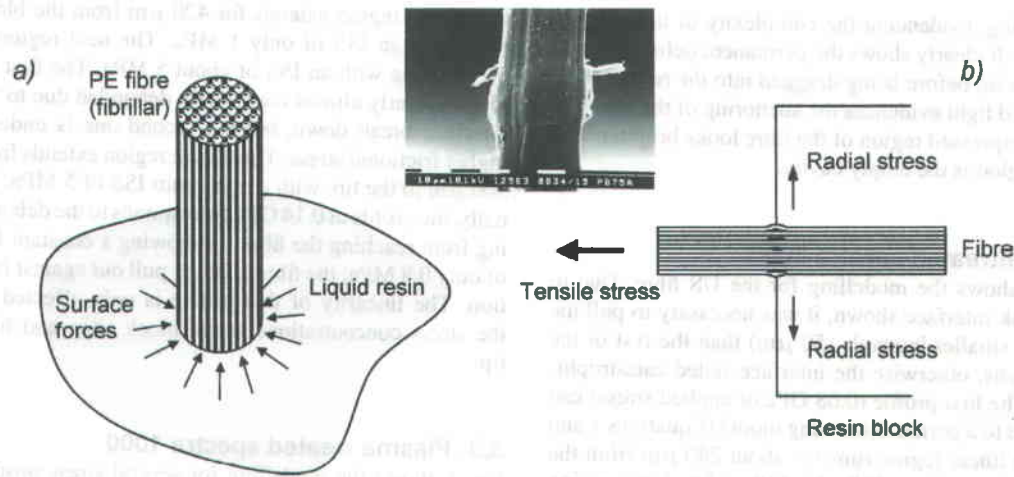


Figure 5 (a) Forces acting around the fibre at the block edge and (b) exploded area after the fibre (US) is fully debonded.

system due to the many irregularities on the fibre surface and once deformed, it is unable to relax as the free fibre does. Fig. 5 presents the micrograph of a fibre after being pulled out from the resin block: the region that originally was in the block edge. The fibre appears to have exploded whereas the extracted region is undamaged and clean. During the specimen preparation the fibre surface tension attracts the resin forming a meniscus. When the fibre is loaded, large tensile forces are generated on the block edge around the fibre at the meniscus. These tensile forces are stronger than the cohesive forces between the fibre fibrils (which are normally weak due to the high molecular orientation in the fibre in its axial direction) producing the fibre splitting in this region [35].

The loading of the free fibre initially made the interface to react elastically. This can be observed in Fig. 4a. The fibre stress has a maximum near the block edge and steadily drops to zero along the fibre body. Higher levels of stress generated a debonding front (Fig. 4b) which travelled along the fibre surface defining two regions: The linear one, near the block edge, governed by friction which corresponds to the debonded section and the elastic region, near the fibre tip, which corresponds to

the bonded section. The profiles at 0.57 and 0.62 GPa of free fibre load, show this transition point at about 700 and 1250 μm respectively.

The stress profile at 0.60 GPa of free fibre stress (Fig. 4b) shows the moment in which the debonding front reaches the fibres tip. There are several well defined linear regions, which indicate that once the interface is debonded, it experienced several different levels of friction along the surface. The profiles at 0.44 and 0.40 GPa of free fibre stress (Fig. 4c) correspond to the fully-debonded fibre being pulled out from the resin against friction showing a perfect linear distribution. Once the interface failed, the stress level on the free fibre dropped, (the interface was unable to resist the applied stress any longer).

The fibre tip shows a peculiar stress distribution in all the profiles (Fig. 4) Before the tip is debonded, the stress increases and then decreases. This was produced by the permanent deformation that the tip suffered as the fibre was cut. When the fibre debonded, the triangular-shaped tip was dragged into the resin cavity, which has a smaller diameter. Consequently, the fibre tip was compressed generating negative stresses in the region (Fig. 4c). Fig. 6 shows the fibre tip before and after

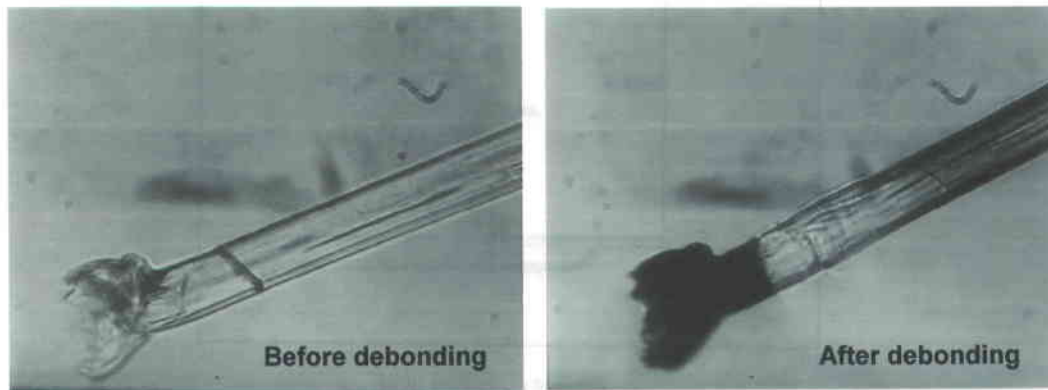


Figure 6 Embedded fibre tip (TS) before and after debonding. The debonded fibre is dragged into the resin cavity, the compressed tip looks bright and the empty cavity looks dark.

debonding, evidencing the complexity of the pull-out process. It clearly shows the permanent deformation at the fibre tip before being dragged into the resin cavity. Polarised light evidences the anchoring of the fibre tip. The compressed region of the fibre looks brighter. The dark region is the empty cavity.

3.2. Untreated spectra 1000

Fig. 7 shows the modelling for the US fibre. Due to the weak interface shown, it was necessary to pull the fibre at smaller intervals ($50\ \mu\text{m}$) than the rest of the specimens, otherwise the interface failed catastrophically. The first profile ($0.08\ \text{GPa}$ of applied stress) can be fitted to a partial debonding model (Equations 1 and 3). The linear region runs for about $280\ \mu\text{m}$ from the block edge with an ISS of $6\ \text{MPa}$. The elastic region shows a maximum ISS of about $6\ \text{MPa}$. As the debonding front travels along the fibre, two linear regions are defined. This is observed at the $0.10\ \text{GPa}$ profile. The

first linear region extends for $420\ \mu\text{m}$ from the block edge with an ISS of only $1\ \text{MPa}$. The next region is $80\ \mu\text{m}$ long with an ISS of about $5\ \text{MPa}$. The first region is clearly almost completely debonded due to the interface break down, but the second one is under a higher frictional stress. The elastic region extends from $500\ \mu\text{m}$ to the tip, with a maximum ISS of $5\ \text{MPa}$. Finally, the profile at $0.14\ \text{GPa}$ corresponds to the debonding front reaching the fibre tip showing a constant ISS of only $0.8\ \text{MPa}$; the fibre is being pull out against friction. The linearity of this profile is only affected by the stress concentrations at the block edge and fibre tip.

3.3. Plasma treated spectra 1000

Fig. 8 shows the modelling for several stress profiles presented in Fig. 4 for the TS fibre. The specimen had a fibre with a long embedded length of about $2500\ \mu\text{m}$. The first profile ($0.45\ \text{GPa}$ of applied stress) shows an

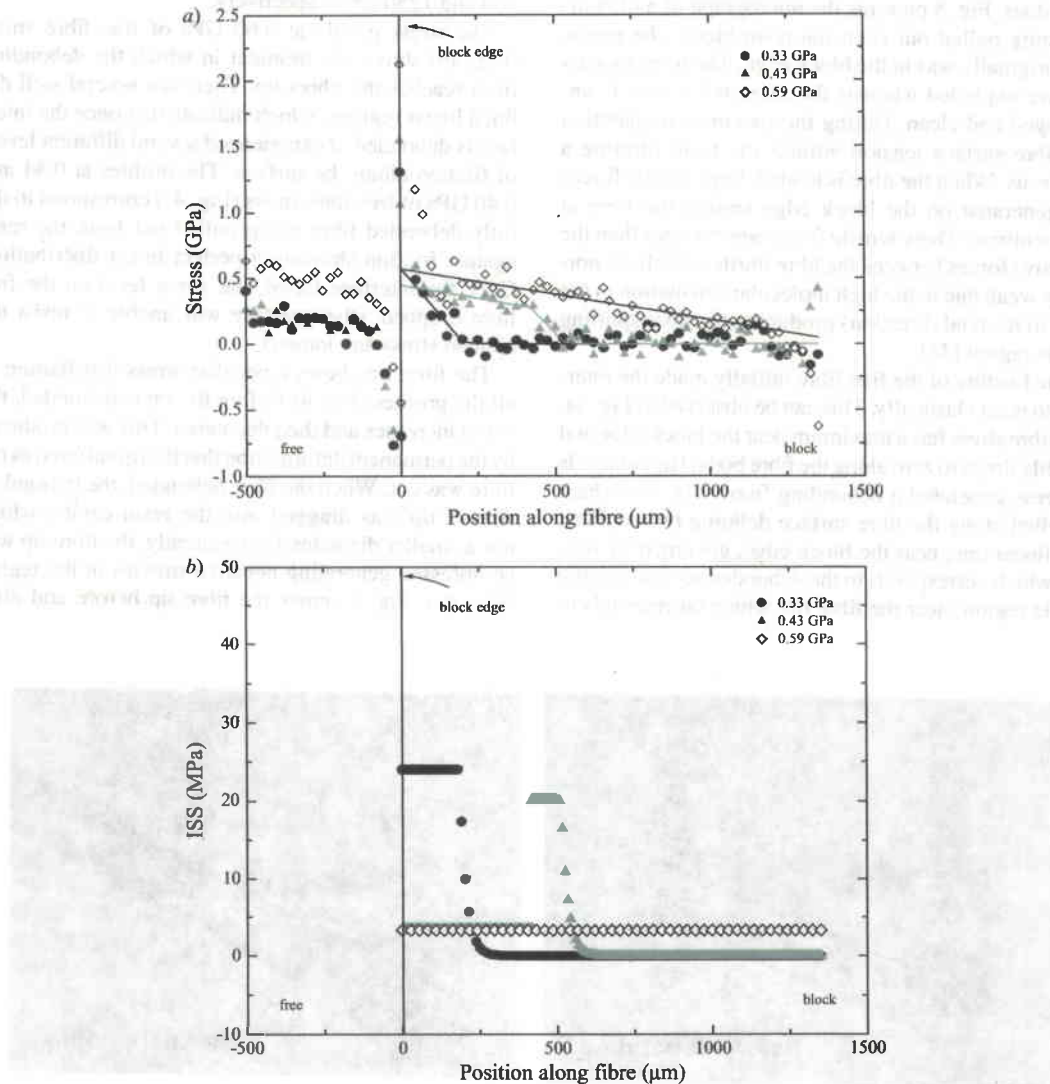


Figure 7 Untreated Spectra 1000 Fibre (US): (a) Raman stress profiles fitted to partial debonding model and (b) ISS profiles calculated from the fitted stress curves.

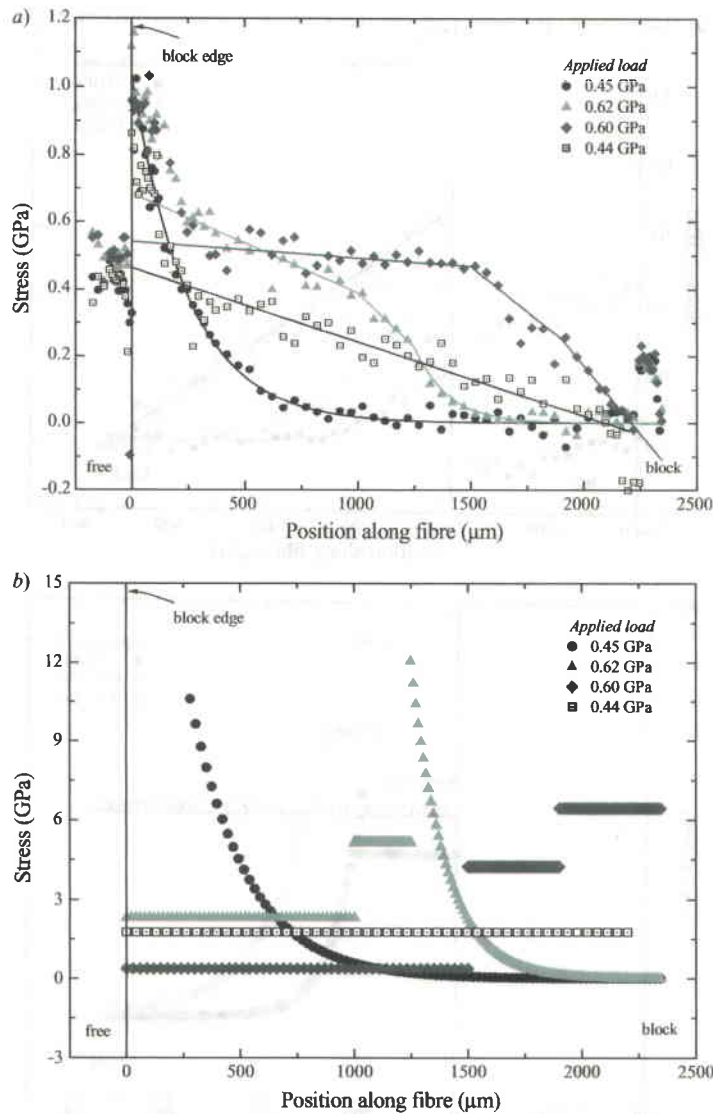


Figure 8 Plasma Treated Spectra 1000 Fibre (TS): (a) Raman stress profiles fitted to partial debonding model and (b) ISS profiles calculated from the fitted stress curves.

elastic response, with a maximum stress at the block edge. The profile shows a strong stress concentration near the block edge (for about 250 μm), which cannot be modelled by a simple force balance (the irregularity affects all the stress profiles). The maximum ISS for the elastic region (11 MPa) is located at 250 μm from the block edge. The second profile (0.62 GPa) shows a partial debonding pattern with two linear regions. The first one (1000 μm long) has an ISS of 2.6 MPa and the second one (250 μm long) has an ISS of 5.7 MPa. The next profile (0.60 GPa) is particularly interesting. The debonding front reached the fibre tip but the fibre is still anchored at its original position. The stress distribution was fitted to 3 different linear regions, indicating that the debonded fibre is subjected to different levels of friction. The lowest one corresponds to the block edge (1500 μm long) with an ISS of 0.5 MPa, which is a fully-debonded region. The following region is 400 μm long with an ISS of 4.4 MPa. The third region has an ISS of 6.4 MPa (400 μm long) and is next to

the hooked tip. When the fibre is finally debonded and dragged along the resin cavity, the frictional ISS along the fibre is constant and equal to 1.7 MPa (profile at 0.44 GPa). The better interfacial adhesion of this fibre (TS), doubled the US interfacial quality (Fig. 7).

3.4. Short embedded lengths

The US fibre was unable to cope with embedded lengths shorter than 1000 μm , the interface failed instantly and catastrophically making the stress mapping impossible. The better adhesion between TS fibre and the Epoxy resin made possible to have shorter embedded lengths. Fig. 9 shows the modelling of the shortest sample tested. The first two profiles show a partial debonding pattern with a debonded region extending up to 200 and 320 μm respectively. The first one shows a constant ISS of about 5.9 MPa and the second one shows a double linear region with 8.8 and 10.2 MPa of ISS. The maximum ISS at the bonded region is 8 and 10.5 MPa respectively. At

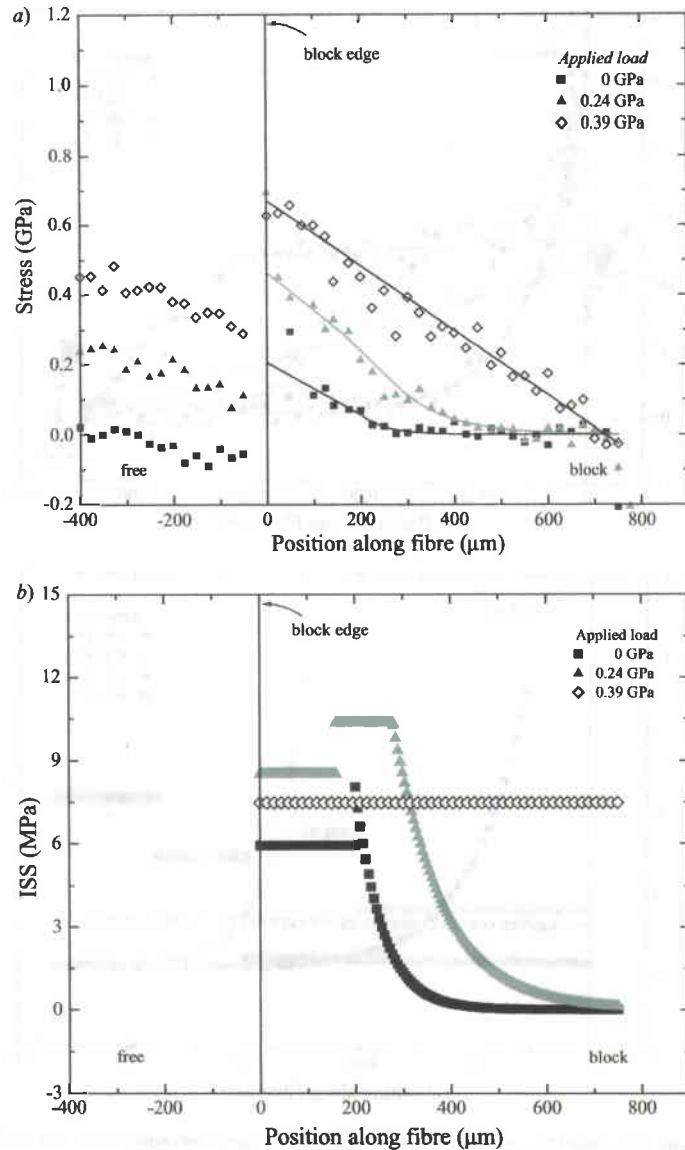


Figure 9 Plasma Treated Spectra 1000 Fibre (TS)—Short embedded fibre: (a) Raman stress profiles fitted to partial debonding model and (b) ISS profiles calculated from the fitted stress curves.

the last profile (0.39 GPa) the fibre is fully debonded with a constant ISS of 7.5 MPa. Comparing these results with the long embedded case (Fig. 8) the levels of ISS are marginally lower but higher than the US case (Fig. 7).

3.5. Chromic treated fibre

The adhesion between the PE fibre and the Epoxy resin was considerably improved by the chemical changes during the fibre surface treatment [31]. This can be observed comparing the UC profiles from Fig. 10 with the US case (Fig. 7). The first difference to notice is the applied stress level at the free fibre, which easily reached 0.24 GPa. Also, the maximum stress on the embedded fibre reached values between 0.20 and 0.40 GPa (US fibre, 0.10–0.25 GPa). The most remarkable difference between them is the good definition of the stress pro-

files of the chromic case. This is a direct effect of the better adhesion between the fibre and the resin. The polar groups attached by the chromic acid treatment to the fibre surface improved the wetting, leading to a closer interaction between the fibre and the resin and consequently to a more efficient and homogeneous stress transfer.

The first profile shown (0.14 GPa of applied stress) has a perfect elastic pattern with a maximum ISS of about 6.30 MPa at the block edge. At this level of applied stress, the US fibre was already debonded (Fig. 7). The second profile (0.24 GPa) shows a partially-debonded pattern; at the block edge, the stress concentration in the region caused a disruption in the profile, which is not predicted by the model. The debonded region extends 300 μm from the block edge showing an ISS of 3.6 MPa. The corresponding elastic region, shows a maximum ISS at 300 μm of about 6 MPa,

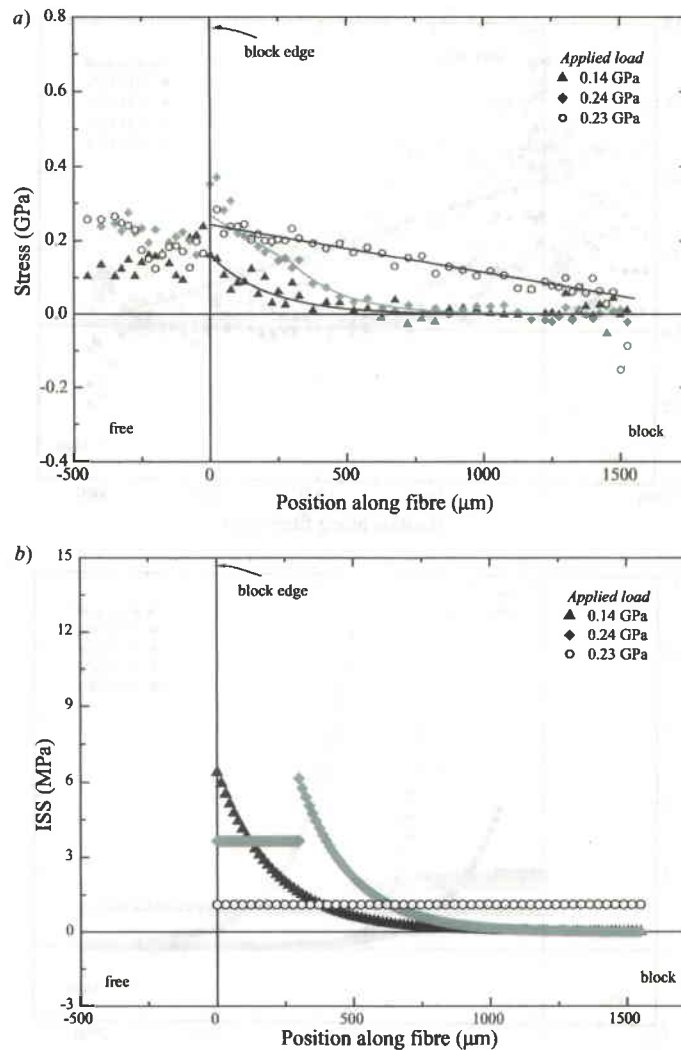


Figure 10 Chromic Treated Spectra 1000 Fibre (UC): (a) Raman stress profiles fitted to partial debonding model and (b) ISS profiles calculated from the fitted stress curves.

which closely matches the ISS of the previous profile. Finally, the profile at 0.23 GPa shows full debonding of the fibre with a constant ISS of only 1 MPa.

3.6. Sulphuric treated fibre

Fig. 11 shows the stress profiles for a pull-out specimen of the TC fibre. They showed the synergic effect of the surface chemistry changes over the interface properties [31]; it was not possible to capture the moment in which the debonding front reached the fibre tip.

The first profile (0.16 GPa) follows a partial-debonding behaviour with a maximum ISS of 5.9 MPa at 200 μm from the edge. The next two profiles (0.23 and 0.51 GPa of applied load) show a debonded region that extends up to 570 and 830 μm respectively, with an ISS of about 2.6 MPa. When the fibre fully debonded, the ISS dropped to 1.6 MPa. The maximum ISS in the bonded region steadily increased with the applied stress from 5.7 to 8.5 and to 13 MPa. All the profiles show a relatively high stress concentration at the block edge due to high levels of friction and also at the fibre end,

caused by the anchoring of the tip [16]. In comparison with the commercial TS fibre (Fig. 8), the synergic effect of the Plasma Treatment and Sulphuric Post-treatment, improve the interface to higher levels. The highest ISS measured by pull-out on the present study was 13 MPa and corresponds precisely to the TC fibre.

4. Conclusions

Raman spectroscopy proved to be able to monitor the fibre interface of a PE/Epoxy composite and to follow the debonding process during a conventional Pull-out Test, which can be summarised as follows: At low levels of applied stress, the system behaves elastically. An increase in the free fibre load generates a debonding front that travels along the fibre/matrix interface. The bonded region still behaves elastically, but the debonded one tends to get longer, with a low ISS as the debonding front propagates along the fibre body. When the debonding front reaches the fibre tip, several linear regions are generated. These linear stress distributions along the fibre are disturbed by high stress

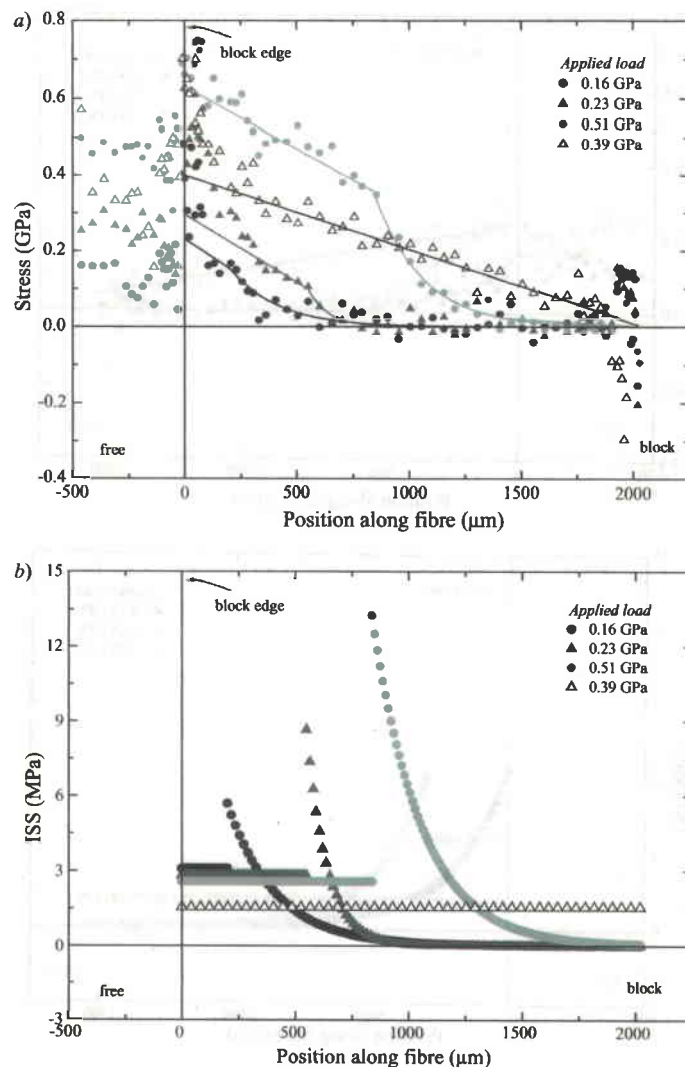


Figure 11 Plasma Treated Spectra 1000 Fibre with sulphuric post-treatment (TC): (a) Raman stress profiles fitted to partial debonding model and (b) ISS profiles calculated from the fitted stress curves.

concentration at the block edge and at the fibre tip. As the fibre starts to pull-out, a low and constant ISS due to friction is observed along the fibre; the interface is totally destroyed.

A large concentration of stress was observed at the block edge caused not only by the surface irregularities of the fibre but also by presence of radial stresses, disturbing all the stress profiles. This region was not possible to fit using a simple force balance, because they represent a more complex phenomenon. The forces are strong enough to open up the fibrillar structure of the fibre. This stress concentration might be generated during the specimen manufacture due to the surface tension of the matrix; as a liquid tends to form a meniscus around the fibre.

Before debonding, the fibre tip shows a singular stress profile due to the permanent deformation caused when the fibre is cut. When the fibre is pulled-out, negative stress values are observed caused by the compression of the fibre tip as it is dragged into a smaller diameter resin cavity—The fibre tip acts as an anchor.

The free fibre also influences the Pull-out process. It relaxes after the stress is applied showing stress levels lower than in the embedded section where the interface irreversibly deforms. Further deformation increases the free fibre stress until the interface fails and no longer resists deformation, then, the stress on the free fibre steadily drops.

Untreated Spectra 1000 (US) showed the weakest interface, requiring long embedded lengths (over 1200 μm) and low levels of stress on the free fibre to be able to observe a steady debonding process. Plasma Treated Spectra 1000 (TS) showed a better interface than US: A maximum ISS ranging between 10 and 12 MPa was observed even for the shortest embedded length tested (750 μm).

The chemical treatments were successful in improving interfacial adhesion. The chromic treatment improved the adhesion of the PE fibre (UC); the interface did not fail as easy as in the Untreated case (US) showing a maximum ISS of 6 MPa (the US fibre had an ISS of about 4.5 MPa at lower levels of applied stress). The

synergic effect of the Plasma Treatment and Sulphuric Acid Treatment on the fibre (TC) increased the interfacial strength to even higher levels. The maximum ISS reached was 13 MPa, which is not only higher than in the Untreated fibre case (US) but also, the highest value obtained in the present work for the PE/Epoxy system (thermoplastic-thermoset interface).

Acknowledgements

P. I. G-Ch. would like to thank to Consejo Nacional de Ciencia y Tecnología (CONACYT) of Mexico for financial support and R. J. Y. is grateful to the Royal Society for Wolfson Research Professorship and to EP-SRC for the support to the overall program of Raman spectroscopy for the analysis of fibre and composite deformation.

References

1. L. J. BROUTMAN, "Interfaces in Composites," ASTM STP452 (1969) p. 27.
2. F. P. M. MERCX and P. J. LEMSTRA, *Polym. Commun.* **31** (1990) 252.
3. B. MILLER, P. MURI and L. REBENFELD, *Comp. Sci. Techn.* **28** (1987) 17.
4. H. D. WAGNER, E. GALLIS and E. WIESEL, *J. Mater. Sci.* **28** (1993) 2238.
5. M. J. PITKETHLY, J. P. FAVRE, U. GAUR, J. JAKUBOWSKI, S. F. MIDRICH, D. L. GALDWELL, L. T. DRZAL, M. NARDIN, H. D. WAGNER, L. D. LANDRO, A. HAMPE, J. P. ARMISTEAD, M. DESAEGER and I. VERPOEST, *Comp. Sci. Techn.* **48** (1993) 205.
6. G. DÉ SARMOT and J. -P. FAVRE, *ibid.* **42** (1991) 151.
7. A. KELLY and W. R. TYSON, *J. Mech. Phys. Solids* **13** (1965) 329.
8. A. KELLY and N. H. MACMILLAN, "Strong Solids" (Clarendon Press, 1986).
9. L. S. PENN and S. M. LEE, *J. Comp. Techn. Res.* **11** (1989) 23.
10. M. R. PIGGOTT, *Comp. Interf.* **1** (1993) 211.
11. M. J. PITKETHLY and J. B. DOBLE, *Composites* **21** (1990) 389.
12. L. C. N. BOUGH, R. J. MEIER, H. -H. KAUSCH and B. K. KIP, *J. Polym. Sci., Part B: Polym. Phys.* **30** (1992) 325.
13. Z. -F. LI and A. N. NETRAVALI, *J. Appl. Polym. Sci.* **44** (1992) 333.
14. D. T. GRUBB and Z. -F. LI, *J. Mater. Sci.* **29** (1994) 203.
15. A. K. PATRIKIS, M. C. ANDREWS and R. J. YOUNG, *Comp. Sci. Techn.* **52** (1994) 387.
16. D. J. BANNISTER, M. C. ANDREWS, A. J. CERVENKA and R. J. YOUNG, *ibid.* **53** (1995) 411.
17. X. YANG, D. J. BANNISTER and R. J. YOUNG, *J. Amer. Ceram. Soc.* **79** (1996) 1868.
18. X. GU, "Micromechanics of Model Carbon Fibre/Epoxy Resin Composites," PhD Thesis, University of Manchester Institute of Science and Technology (UMIST) 1995.
19. B. J. KIP, M. C. P. VAN EIJK and R. J. MEIER, *J. Polym. Sci., Part B: Polym. Phys.* **29** (1991) 99.
20. J. A. H. M. MOONENE, W. A. C. ROOVERS, R. J. MEIER and B. J. KIP, *J. Polym. Sci., Polym. Phys.* **30** (1992) 361.
21. D. T. GRUBB and Z. -F. LI, *Polymer* **33** (1992) 2587.
22. S. VAN DER ZWAAG, M. G. NORTHOLT, R. J. YOUNG, I. M. ROBINSON, C. GALIOTIS and D. N. BATCHELDER, *Polym. Commun.* **28** (1987) 276.
23. R. P. WOOL, R. S. BRETZLAFF, B. Y. LI, C. H. WANG and R. H. BOYD, *J. Poly. Sci.: Part B: Polym. Phys.* **24** (1986) 1039.
24. M. R. PIGGOTT, "Load Bearing Fibre Composites" (Pergamon Press, Oxford, UK, 1980) p. 83.
25. P. S. CHUA and M. R. PIGGOTT, *Comp. Sci. Techn.* **22** (1985) 33.
26. M. R. PIGGOTT, *ibid.* **42** (1991) 57.
27. T. LACROIX, B. TILMANS, R. KEUNINGS, M. DESAEGER and I. VERPOEST, *ibid.* **43** (1992) 379.
28. "Ciba-Geigy Data Sheet," Publication No. s.90a, May, 1988.
29. M. C. ANDREWS, "Stress Transfer in Aramid/Epoxy Model Composites," PhD Thesis, University of Manchester Institute of Science and Technology (UMIST) 1994.
30. P. I. GONZÁ LEZ-CHI, "Deformation Micromechanics in Polyethylene-Epoxy Fibre-Reinforced Composites," PhD Thesis, University of Manchester Institute of Science and Technology (UMIST) 1994.
31. M. NARDIN and I. M. WOOD, *Mater. Sci. Techn.* **42** (1991) 814.
32. S. KUMAR, *Ind. J. Fibre Textile Res.* **16** (1991) 52.
33. Z. -F. LI and D. T. GRUBB, *J. Mater. Sci.* **29** (1994) 189.
34. C. GALIOTIS, R. J. YOUNG, P. H. J. YEUNG and D. N. BATCHELDER, *ibid.* **19** (1984) 3640.
35. C. MAROTZKE, *Comp. Sci. Techn.* **50** (1994) 393.

Received 20 February 2003
and accepted 28 May 2004

